PNAS RESEARCH ARTICLE | DEVELOPMENTAL BIOLOGY OPEN ACCESS

Electrical stimulation promotes longevity and regeneration in a colonial chordate

Jos Domen[a,b,1,2], Yotam Voskoboynik[c], Tom Levy[a,b], Erica M. Domen[d], Katherine J. Ishizuka[a,b], Karla J. Palmeri[a,b], Chiara Anselmi[a,b], Thomas Rolander[a], Norma F. Neff[e], Angela M. Detweiler[e], Irving L. Weissman[b,1,2], Kimberly L. Gandy[a,1], Debashis Sahoo[f,g,1,2], and Ayelet Voskoboynik[a,b,1,2]

Affiliations are included on p. 9.

Contributed by Irving L. Weissman; received March 27, 2026; accepted April 20, 2026; reviewed by Loriano Ballarin and Erez Braun

Endogenous bioelectric currents regulate development and regeneration, but their influence on organismal longevity and stem cell–mediated repair is not well understood. We demonstrate that a brief, clinically safe pulse of electrical current (PEC) produces lasting rejuvenation in the colonial chordate *Botryllus schlosseri*. In this species where all differentiated tissues are replaced weekly and progenitor populations mediate the weekly de novo generation of new organs, organismal aging is directly driven by alterations of the precursor pool. Electrically stimulated colonies exhibited increased growth, enhanced reproductive activity, and significantly improved survival, along with improved stem cell associated function. Whole-transcriptome analysis revealed a biphasic "reboot and rebound" program across all functional paths. An acute 2-h "reboot" was defined by the synchronized downregulation of the genomic engine, mitochondrial respiratory chain, contractile apparatus, and extracellular matrix (ECM) integrity. This systemic pause transitioned into a massive 24-h "rebound", characterized by the global reactivation of these paths, including a metabolic surge, cytoskeletal rebuilding, and ECM scaffold synthesis. Notably, PEC induced a conserved immunometabolic shift from a proinflammatory to a reparative signature, mimicking exercise-induced shifts observed in mammals. Our findings identify that PEC acts directly on progenitor-cell-driven pathways to restore homeostatic vitality, offering insights into the reversal of age-related decline.

pulsatile electrical current | rejuvenation | stem cell aging | longevity | tunicate

Significance

Aging is characterized by the progressive loss of stem cell function and tissue homeostasis. Using the invertebrate chordate *Botryllus schlosseri*, we demonstrate that brief pulsatile electrical current (PEC) induces long-lasting rejuvenation. In this species, where tissues are replaced weekly, most likely via stem cell–mediated de novo organogenesis, PEC stimulation enhances growth, fertility, and survival. Transcriptomic analysis suggests this is driven by a coordinated "reboot" of metabolic and genomic paths, followed by a high-fidelity homeostatic state. This signature mirrors immunometabolic shifts observed in mammals after exercise. Posttreatment upregulation of epigenetic regulators in both young and old cohorts suggests a mechanism for stabilizing the rejuvenated genome, raising the possibility that related bioelectrical strategies may improve health and resilience in mammals.

Naturally occurring bioelectric currents are critical for development and regeneration, with all cells generating electrical networks that control gene expression and behavior (1–4). This principle extends from *Planaria, Hydra,* and salamanders where electric currents are critical for regeneration, to mammals, where electrical stimulation shows promise in modulating neural stem cells and treating nerve and spinal cord injuries (5–9). Clinically, externally generated currents aid wound healing, immunomodulation, and tissue repair (10–13). Despite extensive research on bioelectrical stimulation, limited data exist on its direct application to influence organismal stem and progenitor-cell-driven regenerative activity, longevity, and fertility. This study addresses this gap by evaluating a reproducible pulsatile electrical current (PEC) regimen. We provide detailed cellular and molecular insights into PEC's effects on cell activity, longevity, and fertility using *Botryllus schlosseri*, a member of the subphylum Tunicata, our closest living marine invertebrate relatives, which in the case of *Botryllus,* exhibits significant sequence similarity to approximately 70% of human protein-encoding genes (14, 15). *B. schlosseri*, offers a great system for studying aging, thanks to its unique life cycle encompassing sexual and asexual reproduction, as well as natural chimera formation (16–22). Each *Botryllus* colony consists of multiple interconnected individuals called zooids, which undergo weekly asexual reproduction. During this process, older zooids are reabsorbed, and new, genetically identical zooids mature from buds. Crucially, our published studies suggest that only the stem cells persist across these weekly regeneration cycles, while all differentiated tissues are replaced (17–19, 22–24). This continuous renewal from a long-lived stem cell pool suggests that the overall aging of the colony is directly driven by the aging of its stem cells, making *B. schlosseri* an exceptional model to understand how stem cell dynamics contribute to organismal longevity and decline (24–27). Indeed, *B. schlosseri* has been successfully used to study stem cell aging and stem cell competition in natural chimeras (16–20, 22, 24, 26–30) with findings that have led to discoveries in their mammalian counterparts (31–37).

B. schlosseri colonies, embedded in a gelatinous tunic, consist of interconnected zooids and buds, forming "flower-like" systems (Fig. 1 *A-D*). Each zooid has a heart that drives circulation through a shared vasculature, terminating in peripheral ampullae. *B. schlosseri* exhibits both well-characterized sexual and asexual reproductive cycles (21, 22). In the

Reviewers: L.B., Universita degli Studi di Padova; and E.B., Technion Israel Institute of Technology.

Competing interest statement: Medronic the company that manufacture the Pacemaker used in this study contributed the pacemakers and electrodes used in this study.

[1]J.D., I.L.W., K.L.G., D.S., and A.V. contributed equally to this work.

[2]To whom correspondence may be addressed. Email: jdomen@stanford.edu, irv@stanford.edu, dsahoo@health.ucsd.edu, or ayeletv@stanford.edu.

This article contains supporting information online at https://www.pnas.org/lookup/suppl/doi:10.1073/pnas.2610968123/-/DCSupplemental.

Published May 26, 2026.

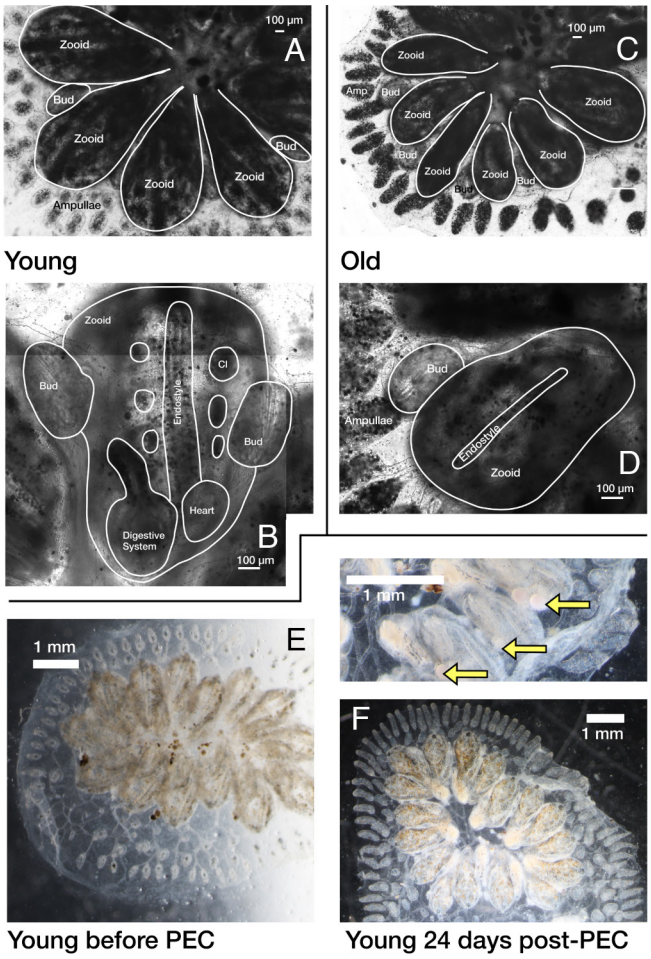

Fig. 1. Age-related morphological changes and PEC-induced rejuvenation in *Botryllus schlosseri*. (*A* and *B*) Live images of a young (2-mo-old) colony. (*C* and *D*) Live images of an old (24-y-old) colony. (*A*) A *Botryllus* colony comprises interconnected zooids, each bearing buds and connected to a shared blood vessels network terminating in peripheral ampullae (Amp). Young colonies (*A* and *B*), exhibit larger sized zooids with less pigmentation compared to old colonies (*C* and *D*), which also show differences in ampullae' morphology, size, and pigmentation (*B*) A young zooid, requiring two 10x magnification images to capture its entirety. Internal organs such as the digestive system, heart, endostyle, and cell islands (CI) can be observed through its semitransparent body. (*D*) An entire old zooid and its buds at the same developmental stage and magnification fit within a single frame, highlighting the significant size reduction in older zooids and their organs (*D* Scale bar is similar to *B* Scale bar). (*E*) A 10-wk-old young colony before exposure to PEC, shows an opaque tunic, retracted and shortened ampullae, and the absence of gonads and embryos. (*F*) The same colony 24 d after PEC exposure shows a transparent tunic, extended ampullae, and embryos and gonads in nearly every zooid (arrows). [Scale bar, 100 µm (*A*–*D*) or 1 mm (*E* and *F*)]. Magnification: A, C: ×4; others: ×10. Zooids, buds, and internal organs are outlined.

asexual cycle, genetically identical zooids mature weekly from buds, replacing older zooids in a takeover process (21, 22, 38). This rapid, consistent asexual cycle allows colonies to be maintained and expanded for decades in the laboratory, making them ideal for long term studies of biological changes. Our lab has cultured colonies for over 24 y, spanning more than 1,000 blastogenic takeovers, enabling direct comparison between young cohorts and extremely long-lived genotypes (Fig. 1 *A*–*D*) (26, 27).

In the reproductive season, sexually mature colonies form gonads. Fertilized eggs then undergo classic chordate development inside the mother colonies, producing larvae that ultimately settle and metamorphose into sessile zooids which will found new colonies (21, 22). As colonies age, both sexual and asexual reproduction slows, demonstrating reduced regenerative potential (25). Aging is also associated with morphological changes, including increased pigmentation, altered blood vessel morphology, and significantly decreased zooid size (25–27) (Fig. 1 *A*–*D*). These changes are accompanied by molecular shifts, such as altered gene expression patterns related to circadian regulation (27). Furthermore, the *B. schlosseri* central nervous system shows age-related declines in neuron numbers and gene expression changes linked to human neural stem cells and neurodegeneration pathways (26). This study demonstrates that PEC profoundly rejuvenates the colonial chordate *B. schlosseri*, leading to significant long-lasting improvements in health, regeneration, reproductive output, and lifespan. These rejuvenating effects are driven by PEC-induced "reboot" of metabolic, contractile, and genomic paths, followed by a high-fidelity homeostatic state. This signature resembles exercise-induced immunometabolic shifts observed in mammals, offering insights into aging and regeneration.

Results

PEC Induced Younger Phenotypes and Increases Regenerative Output. We delivered PEC to mouse embryonic stem cell–derived cardiomyocytes using a Medtronic 5375 pacing device and observed that the contraction frequency of cardiomyocyte patches synchronized to the frequency set on the device (*SI Appendix*, Fig. S1*B*). Hypothesizing that increased or coordinated heart contractions and improved circulation might alter biological properties, we applied this system to *B. schlosseri*. Initial observations showed that PEC treatment caused unhealthy or older animals to assume a younger phenotype, noticeable within 48 h. Within a few weeks poststimulation, these animals exhibited features characteristic of younger individuals, including lighter pigmentation, larger zooids, more elongated ampullae extending to the tunic edge, a clearer tunic, and increased gonad production (Fig. 1 *E* and *F*). For PEC application, we used a Medtronic 5375 pulse generator, a device developed for clinical cardiac surgery (*SI Appendix*, Fig. S1*A*). Our PEC regimen was developed based on existing clinical knowledge of safe and effective voltage and frequency parameters employed in cardiac pacing. To evaluate various PEC regimens for *B. schlosseri*, we pulsed animals at 20 mA and 150 pulses per minute (ppm), a rate faster than the typical *B. schlosseri* heart rate of 60 to 90 beats per minute (bpm) (27). Pulsing duration ranged from 5 min to 16 h. After evaluating pilot experiments (*SI Appendix*, Table S1), we selected a regimen of 20 mA, 150 ppm for 5 min, repeated three times with 20-min intervals for subsequent studies. For some initial experiments, the same 20 mA, 150 ppm for 5 min was applied six times with 48-h intervals. Exact dates of settling (DOB) and date of treatment for the various experiments are listed in *SI Appendix*, Table S1. In our experiments, colonies were considered young if maintained in culture for no more than 18 mo after initial settling and metamorphosis into oozoids. The two old colonies analyzed had been cultured for 14 and 24 y respectively.

PEC Increases Regenerative Output and Lifespan. We investigated whether the positive effects of PEC correlated with heart rate changes in *B. schlosseri*. Our findings show that PEC-treated colonies (3x5min) exhibited an increased heart rate 1 to 2 h following stimulation, a change that persisted, albeit to a lesser extent, up to 18 d after treatment (Fig. 2*A* and Movies S1 and S2). Furthermore, PEC significantly enhanced regenerative activity in young colonies, with treated colonies producing considerably more buds and zooids by day 23 compared to controls (Fig. 2*B*). Notably, late in the fall gonads were observed in 7 out of 9 treated colonies compared to only 1 out of 9 untreated controls, $P = 0.0115$ (Fisher exact test, Fig. 2*C*).

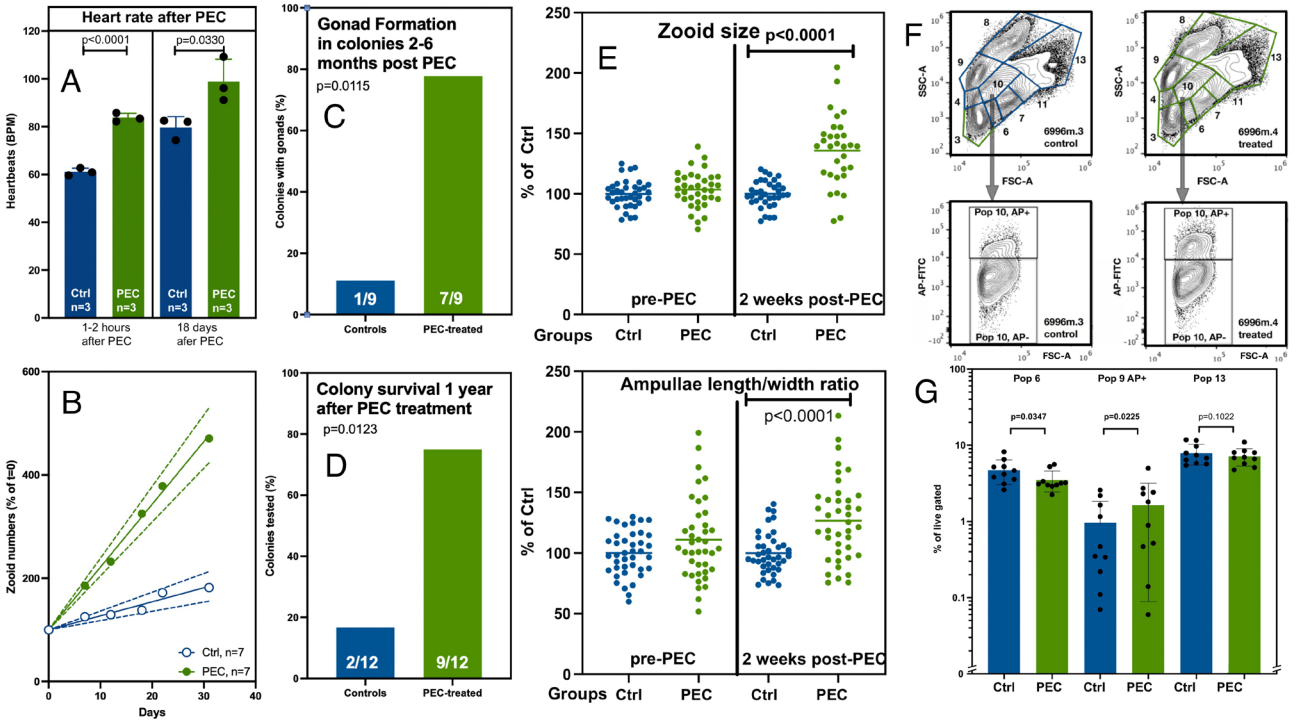

Fig. 2. PEC treatment enhances physiological function and cellular composition in young colonies. (*A*) Comparison of heartbeat frequency between control and PEC-treated colonies (3 × 5min) on the day of treatment (*Left*) and 18 d after treatment (*Right*). Data are presented as average ± SD. (*B*) Average zooid numbers over 35 d for 7 untreated control colonies and 7 PEC-treated colonies as detailed in *SI Appendix*, Table S1 (4 to 5 mo old at treatment). Zooid numbers in treated colonies are significantly higher on days 20 and 25 following treatment. (*C*) Proportion of zooids with gonads in treated and control animals 2 to 4 mo posttreatment. More treated animals developed gonads late in the season (August–November), and in most of their zooids. (*D*) Survival rates of 12 control and 12 treated colonies one year after treatment, showing significantly higher survival of treated colonies (*SI Appendix*, Table S1). (*E*) Average zooid area and ampulla length/width ratio measured using ImageJ two weeks after treatment. Data are shown from 4 colonies per group (*SI Appendix*, Table S1), with 10 measurements per colony. Values are normalized to the control group $^{**}P < 0.0001$. (*F*) Flow cytometric evaluation: Gating setup according to Rosental et al. (39). Gates are based on scatter parameters, propidium iodide staining (dead cell exclusion), and a fluorescent substrate for alkaline phosphatase (AP-FITC). X axis shows populations as defined by Rosental et al. (39), Y axis the percent of live-gated events in that gate. (*G*) Comparison of several blood cell populations between control (blue bars) and PEC-treated (green bars) 4 wk posttreatment. Live gated is gated for scatter parameters and negative for propidium iodide staining. Differences reaching significance were observed in population 6 and population 9 AP^+ (contains Morula cytotoxic cells). Comparisons in panels *A*–*E* are analyzed with a two-tailed unpaired *t* test, G with a paired *t* test.

PEC treatment also led to increased lifespans and rejuvenated health indicators. At 12 mo poststimulation, 9 out of 12 stimulated colonies were still alive, undergoing weekly budding cycles, compared to only 2 out of 12 control colonies ($P = 0.0123$, Fisher's Exact Test) (Fig. 2*D*). PEC also resulted in more robust blood flow within colonies and reduced hyperpigmentation, particularly in the ampullae (Movies S1 and S2). Critically, the size and length/width ratio of zooids and ampullae were significantly larger in PEC-treated colonies compared to controls ($P < 0.0001$) (Fig. 2*E*), consistent with phenotypes observed in younger animals (Fig. 1).

PEC Rejuvenates Aged Colonies. PEC applications significantly improved the morphology and circulation in aged *B. schlosseri* colonies (14 and 20 to 24 y old), effectively reducing hyperpigmentation and increasing regeneration activity as evident by buds and zooids numbers to levels typically found in younger organisms (Fig. 3). For example, Fig. 3 *A*–*C* illustrates the profound effects of PEC on a 24-y-old colony (944axBYd196-6-4), while panels 3D-G show similar data for a 14-y-old colony (SC109e). It is noteworthy that these older colonies typically regenerate smaller zooids compared to young colonies (as demonstrated in Fig. 1 *A*–*D*; using untreated 944axBYd196-6-4). However, following PEC treatment, the size of these older zooids significantly increases (Fig. 3 *C* and *F*). As expected, size increase following PEC is more pronounced for the 24 y old colonies than for the 14 y old colonies which have been cultured for a full decade less. These older colonies were not scored for gonad production. Clone 944, in culture for 24 y, has not produced gonads in at least 15 y, and was not observed to do so following PEC. Experiments with SC109 were done recently and not followed for gonad production.

PEC Alters Immune Cell Populations. To investigate whether PEC leads to significant changes in *Botryllus* cell populations we employed flow cytometry, building on previously characterized stem-cell and immune cell-containing populations in *B. schlosseri*, identified using propidium iodide (PI), size, granularity, and a FITC-labeled substrate for Alkaline Phosphatase, an enzyme known to be expressed at high levels in stem cells (39, 40). FSC/SSC gating indicates that while zooid size increases following PEC, as shown in Fig. 2*E*, cell size does not (Fig. 2*F*). Gating for *B. schlosseri* cell populations (39) in a control colony and a PEC-stimulated colony is shown in Fig. 2*F*. Our analyses revealed significant changes in populations of immune cells, including phagocytes and cytotoxic cells, two months after PEC stimulation. Young animals have significantly higher numbers of AP^+ cells in population 9 post-PEC (Fig. 2*G*; $P < 0.05$) while old animals have lower numbers (Fig. 3*G*). This population encompasses morula cells, which are implicated in cytotoxic activity within *B. schlosseri* colonies (39, 41). Significant changes are also seen in population 6, which contains lymphocyte-like cells (39), and population 13, which contains phagocytic cells (Figs. 2*G* and 3*G*). While our flow cytometry analyses suggest PEC-induced changes in specific cell populations, the current lack of *Botryllus*-specific antibodies and

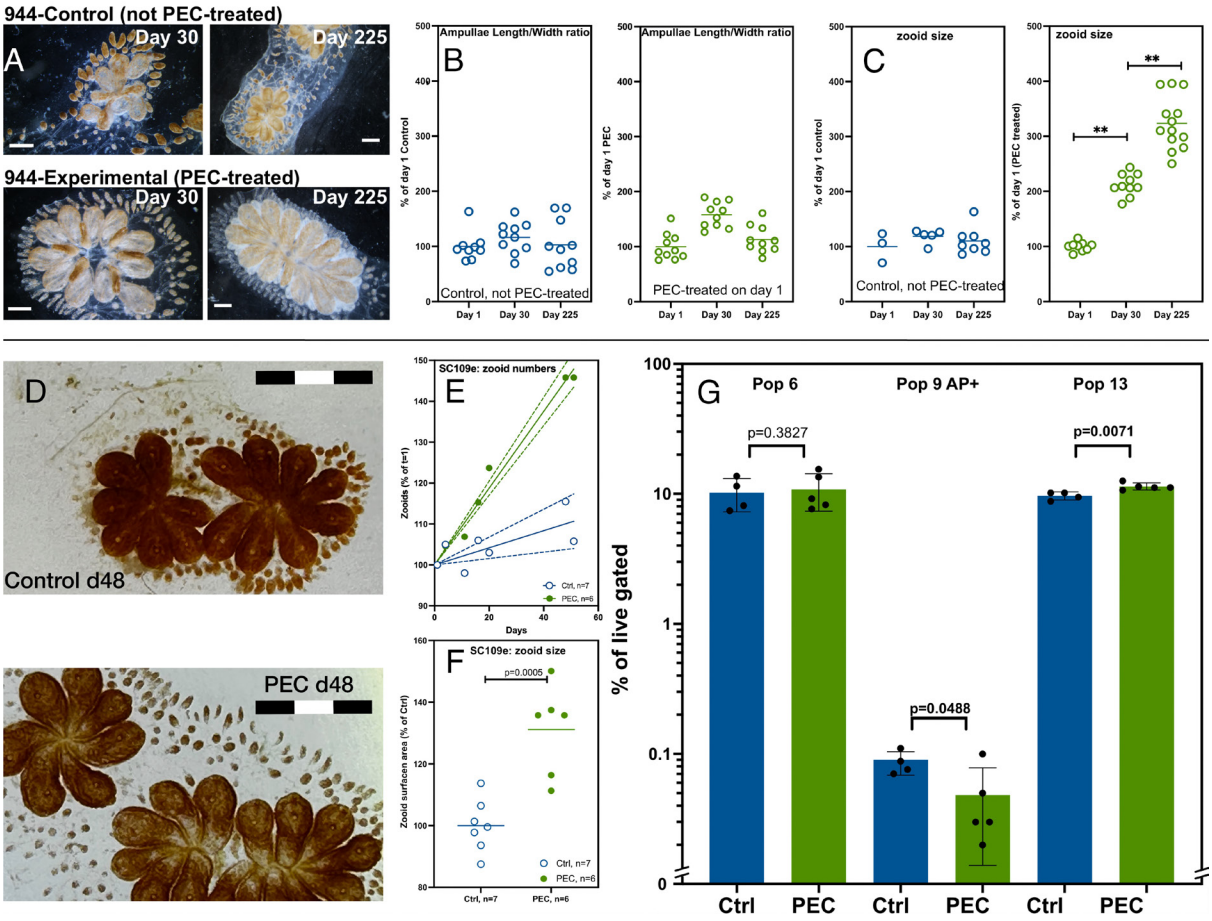

Fig. 3. PEC treatment rejuvenates aged *Botryllus* colonies. (*A*–*C*) Effects of PEC treatment on colony 944axBYd196-6-4, 20+ y old in mariculture. (*A*) Prior to PEC treatment this colony was in poor condition (criteria as in Fig. 1). A single PEC treatment resulted in clear short-term and long-term improvements. (Scale bar, 1 mm.) (*B*) The length/width ratio for the ampullae does not change significantly long-term. Data from 10 ampullae per treatment. Normalized to the day 1 value. (*C*) Zooid size increased significantly after PEC treatment (**$P < 0.0001$). Data from 3 to 13 zooids per colony at different timepoints, as detailed in *SI Appendix*, Table S1. Normalized to day 1 value (*D*–*G*) Effects of PEC on SC109e (14 y old) n = 7 (control) and n = 6 (treated) animals per group. (*D*) Morphology of subclones of SC109e on day 48 after PEC treatment versus control. (Scale bars are in mm.) (*E*) Zooid number and (*F*) size in control and treated SC109e subclones. Size was determined 48 d after PEC treatment. Zooid size normalized to control value. Dashed lines indicate 95% CI. PEC treatment at t = 0. (*G*) Flow cytometry analysis (gating as in Fig. 2*F*) of SC109e, 7 wk posttreatment. Live gated is gated for scatter parameters and negative for propidium iodide staining. Similar to young colonies (Fig. 2) there are no major changes seen following PEC-treatment. PEC-treated animals may have less AP+ cells in population 9 (which contains Morula cytotoxic cells). Population 13 (which contains phagocytic, macrophage-like cells) may have expanded. Analysis of 4 control colonies and 5 PEC treated colonies.

the inherent rarity of stem cells in general circulation limits the resolution of these assays to major changes in larger populations.

PEC Triggers Lasting Transcriptomic Reprogramming. To evaluate genes affecting rejuvenation, we performed whole-transcriptome sequencing on 47 samples from young (373–465 d old) and old (7,668 d old) *B. schlosseri* colonies (42) (SI1; Fig. 4). PEC-treated and control colonies were compared using identical genotypes at each time point, with all samples collected at the same blastogenic phase and time posttreatment. Young colonies were sampled at 2 h (n = 12), 24 h (n = 12), 13 and 49 d (n = 8), and 132 d (n = 6). Due to the extreme 21-y age of the old colonies, only a single genotype was available for testing at 24 h (n = 5), 41 d, and 93 d (n = 5). By comparing clones of the same genotypes within both groups, we ensure that the observed transcriptomic shifts represent authentic PEC-related responses rather than intergenotypic variation.

The Young Colony Response: Systematic Rejuvenation Through Acute Flux. The transcriptomic response in young colonies follows a distinct "reboot and rebound" pattern. During the acute 2-h phase, colonies undergo a profound transcriptomic "reboot", characterized by the downregulation of 237 genes against only 43 upregulated genes (Fig. 4*A* and *SI Appendix*, Fig. SI1). This phase is anchored by the simultaneous suppression of several functional hubs: master transcription factor genes (*Sox2*, *Sox11*), epigenetic regulator genes (*Crebbp*), and the physical silencing of the genome via RNA Polymerase (*Pol*) and DNA repair enzyme genes (*Lig3*, *Prkdc*). Parallel to this, environmental communication is severed through the loss of core kinase genes (*Atr*, *Pi3k*) and internal logistic genes (*Arf1/3*, *Snx27*, *Cul3*). Metabolic suppression follows, involving the mitochondrial respiratory chain and *Tca* cycle genes (*Cyc1*, *Nduf22*, *Pdha1*), while the contractile and ciliary apparatus is disabled via the *Myo10*, *Myl6/10 genes*, and dynein genes (*Dnah5/7/14*). Finally, tissue integrity is destabilized by the reduction of ECM "glues" and receptor genes (*Col5a1*, *Hmcn1/2*, *Lrp1b*). This stage is marked by regulatory pause and presents an epigenetic "clean slate".

While largely suppressive, the 2-h phase includes a selective "triage" response of 43 upregulated genes focused on survival and quality control. Signaling shifts toward membrane dynamics (*Lphn2*, *Bai2*, *Lrp2*, *Abi2*, *Lrig3*) and the activation of *Nos1*, a likely biochemical transducer of the initial stimulus. Mitochondrial

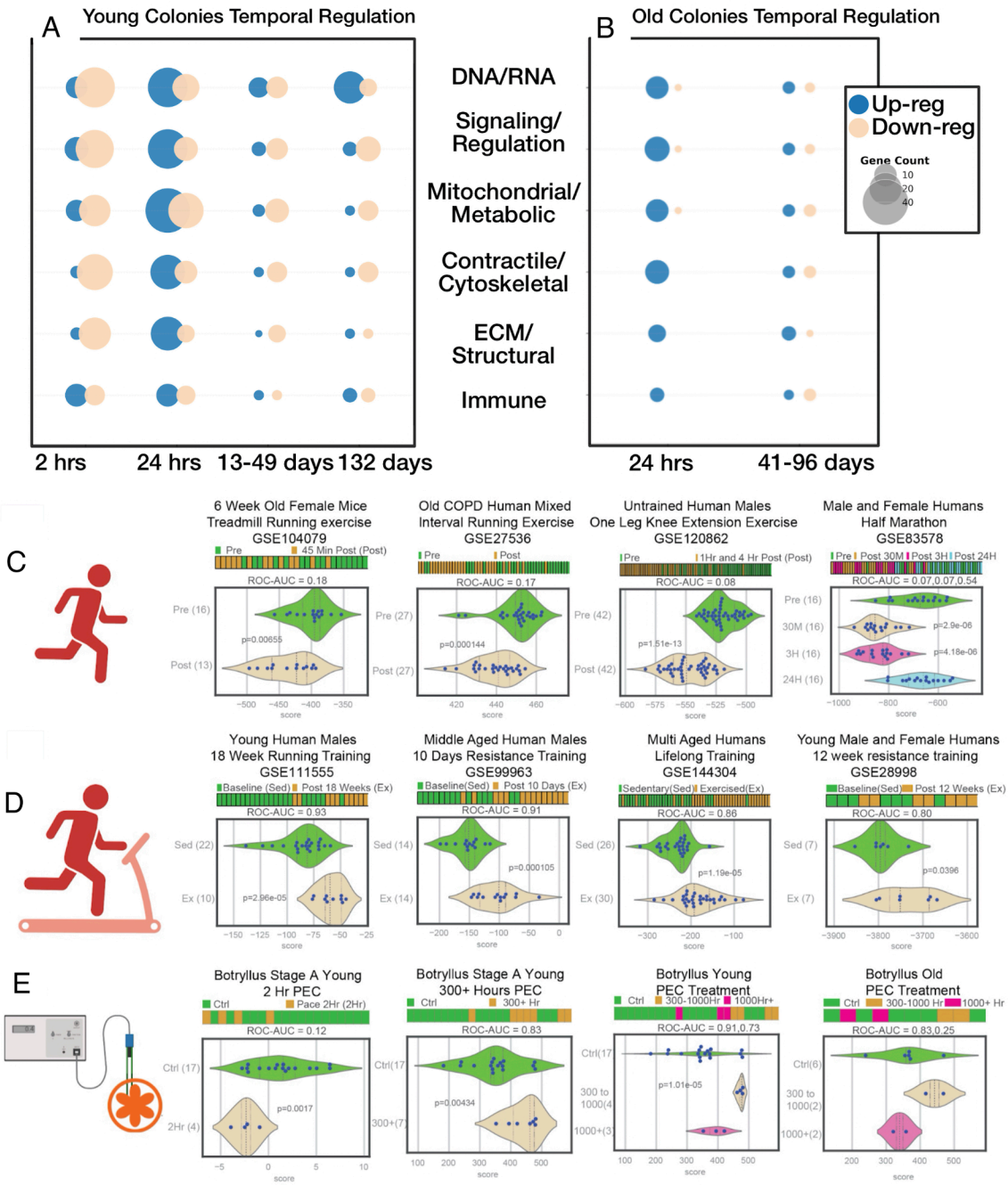

Fig. 4. Global transcriptomic "reboot and rebound" programs following PEC treatment. (*A*) Young cohorts (n = 38; ages 373 to 515 d). Bubble plots represent the volume and direction of differentially expressed genes (DEGs) across four posttreatment time points (2 h, 24 h, 13 and 49 d, 132 d), as determined by DEseq2 analysis (P <= 0.05; |Log2FC|> 1). Each bubble corresponds to a functional "hub", with the bubble diameter proportional to the number of genes identified within that category. The acute 2-h phase reveals a systemic transcriptomic "reboot" defined by the coordinated downregulation (pale orange bubbles) of genomic, metabolic, contractile, and ECM hubs. By 24 h, a massive "rebound" is observed through the global upregulation (blue bubbles) of biosynthetic and structural machinery. Longitudinal sampling (13 to 49 and 132 d) illustrates a transition into a high-fidelity homeostatic state. (*B*) Old cohorts (n = 9; age 7,667 to 7,788 d). Functional hub analysis for the extremely long-lived genotype (21 y in culture). At 24 h post-PEC, old colonies exhibited a constructive upregulation of genes associated with genomic, metabolic, contractile, and ECM hubs dominated by cytoprotective and structural hubs. Details regarding RNASeq annotation and DEGs are available in *SI Appendix*, Table S2. (*C*–*E*) proimmune versus cell-repair transcriptional profiles were analyzed using a 338-genes model (proimmune (M1): 48 genes; cell-repair (M2): 290 genes (43, 44), with 13 proimmune and 133 cell-repair *Botryllus* homologs (based on sequence similarities). proimmune-associated genes were assigned negative weights, and cell-repair-associated genes were assigned positive weights. Each sample was assigned a score based on the sum of the average z-score multiplied by the weight of all the model genes, allowing for comparison relative to controls. Thus, higher proimmune gene expression resulted in lower scores, while higher cell-repair gene expression resulted in higher scores. (*C*) In humans and mice, 6 h postexercise, scores were significantly lower compared to unexercised controls, indicating an early proimmune (M1) shift. (*D*) In humans, at least 48 h postexercise, scores were significantly higher than unexercised controls, indicating a sustained cell-repair (M2) signature shift. (*E*) *Botryllus* exposed to PEC exhibited similar transition patterns. In young colonies, 2 h post-PEC, scores were significantly lower than controls, indicative of a proimmune phenotype. At least 300 h post-PEC in all young samples, scores were significantly higher compared to controls, indicative of a cell-repair-associated signature. The strongest cell-repair signal was observed between 300- and 1,000-h post-PEC, declining to control levels thereafter. This pattern was observed in both young and old colonies, although statistically significant only in young colonies (likely due to larger sample size). The y-axis displays the experimental groups, including the number of samples within each group. *P*-values are shown for significant samples. Complete proimmune and cell-repair Botryllus-associated gene lists are available in *SI Appendix*, Table S2. *C* and *D* adopted from (43), *E* displays RNAseq data from 17 young control samples (4 genotypes) and 18 young PEC treated samples (4 genotypes). The rightmost plot presents data from 6 control and 4 PEC treated samples, all derived from a 21-y-old 944 colony.

health is prioritized via the *Sco2*, *Immp2l*, and *Mgst1* genes, while genomic stability is maintained by *Gtsf1*, *Mael*, and *Ddx31*. Early structural adjustments (*Mfge8*, *Hmcn1*, *Slc12a2*) facilitate rapid cell–matrix communication and osmotic balance.

By 24 h, the transcriptome enters a massive regenerative "rebound" characterized by the upregulation of 252 genes compared to 93 downregulated genes (Fig. 4*A* and *SI Appendix*, Fig. SI1). Energetic restoration is driven by the reactivation of the electron transport chain genes (*Ndufa6*, *Ndufs7*) and TCA cycle genes (*Idh3a*, *Agk*). This surge fuels a broad expansion of biosynthetic process genes, including retinoic acid signaling (*Aldh1a2*), lipid remodeling (*Degs1*, *Pla2g4a*), and nutrient transport (*Slc5a12*, *Slc23a2*). Simultaneously, master TFs (*Sp9*, *Znf236*, *Zscan2*) and epigenetic remodelers (*Basz2b*, *Ncor1*) "open" the genome for physical rebuilding. This stage is marked by the comprehensive recovery of the contractile apparatus (*Ttn*, *Myh2*, *Tnnc2*), ciliary machinery (*Dnah5/9*, *Dnaaf1*), and foundational ECM/tight junction genes (*Col12a1*, *Fbn1/2*, *Cldn1/19*).

At the 13 to 49 d interval, young colonies transition from active regeneration to specialized maintenance (Fig. 4*A* and *SI Appendix*, Fig. SI1). Upregulated genes focus on stabilizing chromatin architecture (*H1F0*, *Phc3*) and optimizing translational machinery (*Eef1d*, *Rpl10*, *Snd1*). Signaling remains focused on endosomal trafficking (*Snx27*, *Trappc1*), while metabolism shifts toward specialized enzymatic activities (*Cbr2*, *Cyp2r1*). Structurally, the colonies prioritize intercellular synchronization via gap junctions (*Gjd2*) and microtubule-based kinetic efficiency (*Tctex1d1*, *Ccdc14*).

Conversely, significant downregulation of other genes such as ribosomal assembly (*Eif3m*, *Rpl34*, *Rplp0*) and RNA processing (*Exosc3*, *Cdc5l*) signals a move away from high-energy protein biosynthesis. This stabilization is mirrored by the dampening of autophagy (*Map1lc3a*), mitochondrial flux (*Uqcrfs1*, *Vdac2*), and basement membrane remodeling (*Nid2*, *Svep1*, *Sele*), reflecting a shift into a stable, homeostatic tissue state.

By 132 d, the young transcriptome reflects long-term physiological robustness (Fig. 4*A* and *SI Appendix*, Fig. SI1). A robust suite of 20 upregulated genes maintains genomic integrity and "housekeeping", led by DNA replication/repair factor genes (*Smc3*, *Gins1*, *Rpa1*) and translational regulator genes (*Rpl11*, *Gspt1*, *Suv420h1*). Proteostatic control (*Psmb6*, *Sil1*) and specialized metabolic activity (*Atp5a1*, *Ivd*) remain high. Notably, the Immune hub genes display a signature (lectin, *Mfge8*, *Plscr1*, *Ptx*) of noninflammatory apoptotic clearance.

Simultaneously, colonies undergo "metabolic cooling", downregulating high-volume ribosomal biogenesis genes (*Rpl17*, *Rpl4*) and growth-related signaling genes (*Casp2*, *Pak1*, *Csk*). The structural apparatus is further streamlined through the reduction of ciliary motility genes (*Dnah17*, *Dnai1*, *Rsph9*) and matrix scavenging genes (*Stab2*, *Tnr*). Collectively, these results demonstrate that four months posttreatment, young colonies have reached a highly efficient, quiescent baseline defined by stringent quality control and metabolic conservation (Fig. 4*A* and *SI Appendix*, Fig. SI1).

The Old Colony Response: Targeted Efficiency. At the 24-h mark, the regulatory landscape of old colonies is characterized by a highly efficient and constructive response, with 58 genes up-regulated and only 3 down-regulated (Fig. 4*B* and *SI Appendix*, Fig. SI1). The transcriptional focus in the old group is concentrated within essential survival and structural hubs. Among genes associated with signaling, there is significant up-regulation of *Grn*, a potent growth factor known to mediate cell survival, wound healing, and lysosomal protein trafficking. Additionally, the inhibitor of apoptosis *Birc6* is activated; this gene is recognized for its role in preventing programmed cell death by inhibiting caspase activity, potentially protecting aging cells from stress-induced apoptosis. Other signaling factors include genes encoding *Klkb1*, involved in surface-dependent activation of blood coagulation and inflammation, and *Ptprk*, which regulates cell–cell adhesion and contact inhibition. Genes associated with contractile and cytoskeletal functions are prominently up-regulated. These include *Ttn*, which provides passive elasticity to muscle-like tissues, and the spectrin gene *Sptan1*, essential for maintaining the stability and plastic deformation of the plasma membrane. We also observe increased transcription of *Myh6* and *Myl10*, components of the motor machinery, alongside multiple entries for *Tubb4b*, which forms the structural basis of microtubules. In the DNA/RNA and epigenetic regulation, old colonies activate machinery for transcript stability and replication, including *Celf1*, which regulates mRNA stability and translation, and *Ehmt2*, a major methyltransferase responsible for histone *H3k9* methylation, a key epigenetic mark for gene silencing and heterochromatin formation. Other up-regulated genes include the DNA replication protein *Rpa2* and the RNA-binding protein *Tial1*, which is involved in the formation of stress granules. Genes associated with mitochondrial and metabolic activity are targeted toward stress management and transport. These include upregulation of *Abcg2*, a member of the ATP-binding cassette transporters that protects cells from oxidative stress by exporting various metabolites, and *Hpgds*, which is involved in the production of *Pgd2*, a mediator of inflammation and smooth muscle contraction.

The suppression in old colonies at 24 h is minimal, involving only three identified annotated factors. These include *Tgs1*, a methyltransferase that modifies the 5' cap of small nuclear and nucleolar RNAs, and *Zfp26*, a zinc finger protein typically involved in transcriptional regulation.

In the long term (41 and 96 d following treatment), up-regulated genes continue to focus on structural and genomic stability (Fig. 4*B* and *SI Appendix*, Fig. SI1). Among genes associated with DNA/RNA regulation, the epigenetic stabilizer *H1f0* (Linker histone H1.0) is activated, mirroring the long-term stabilization seen in younger colonies. This is accompanied by *Luc7l2*, a regulator of alternative splicing. Genes associated with the ECM and structural adhesion remain active, including the integrin *Itgb3*, which mediates cell-to-matrix interactions, and *Mfge8*, which is involved in the phagocytic clearance of apoptotic cells and cell–cell adhesion. Genes associated with contractile function, such as *Actn3*, also remain elevated to support mechanical integrity. Among genes that are down-regulated at this stage are *Svep1*, a large adhesion molecule, and metabolic factors such as *Dhrs4* and *Gstm1*. We also observe the suppression of *Camsap3*, which is involved in microtubule organization, and *Rac1*, a small GTPase that regulates the actin cytoskeleton and cell motility.

Age-Independent Convergence on Core Regulatory Hubs and Long-Term Epigenetic Changes. The comparative transcriptomic analysis of young and old colonies reveals a shared regenerative blueprint executed with distinct age-related kinetic and metabolic priorities (Fig. 4 and *SI Appendix*, Fig. SI1). At the 24-h "rebound" phase, both cohorts demonstrate a universal commitment to physical restoration, characterized by the massive reactivation of the contractile apparatus, specifically through the upregulation of *Ttn* and *Myl10*, and a restarting of the genomic engine via RNA Polymerase. While both ages prioritize survival through antiapoptotic signaling (*Birc6*), their metabolic strategies diverge; young colonies drive a surge in mitochondrial biogenesis and nutrient transport, whereas old colonies focus on lipid processing via the Acot family and antioxidant defenses like *Gstt1*.

This divergence persists into the long-term maintenance phase, where the old group (41 to 96 d) continues to reinforce actomyosin motility and specialized ion transport (*Slc34a2*), while the young group (13 to 132 d) transitions more rapidly into a state of high-fidelity immune surveillance and intracellular transport. Despite these temporal differences, both age groups converge on a final homeostatic strategy defined by "biosynthetic cooling", marked by the systemic downregulation of translational machinery such as *Sf3a2*, *Eef1b*, and *Eif3m*, and the stabilization of the rejuvenated genome through the sustained upregulation of the linker histone *H1f0*. Ultimately, these data suggest that while the initial regulatory response may differ in magnitude, both age groups utilize a conserved suite of structural and epigenetic tools to transition from an acute regenerative state into a stable, homeostatic baseline.

PEC Mimics Exercise-induced Immune/Cell-Repair Transcriptome Changes Observed in Mammals. In previously reported mammalian studies (humans, rats, and mice), exercise triggers a transient, proimmune gene signature within hours, which transitions into a sustained, cell-repair-signature observed during the recovery phase (43). Violin plots in Fig. 4 *C–E* display this transition, representing the analysis of 338-gene sets that identified proimmune versus cell repair states, as previously defined (43, 44). This shift involves a transition from an initial proinflammatory state observed within 6 h postexercise in mammals (Fig. 4*C*), to a subsequent reparative state that favors tissue repair, occurring 48 h and beyond postexercise (43) (Fig. 4*D*). PEC treatment abruptly increases the heart rate of *B. schlosseri* above its normal rate of 60 to 90 bpm, consistent with what organisms may experience with exercise. In our *B. schlosseri* model, 112 of the 338 proimmune/cell-repair state genes had identifiable homologues (SI1). Comparative analysis reveals that 2 h after PEC stimulation, *B. schlosseri* exhibited an initial proimmune-like transcriptome signature Fig. 4*E* (column 1) similar to the early response seen in humans after exercise (Fig. 4*C*). Subsequently, *B. schlosseri* transitions to a cell-repair like phenotype by approximately 300 h post–PEC treatment (Fig. 4*E*) (column 2). This transition to a cell-repair state, which mirrors that observed in humans after exercise (Fig. 4*D*), occurred in both young (Fig. 4*E*, columns 2 and 3) and old colonies (Fig. 4*E*, column 4). For both age groups, this cell-repair signature persisted from 300 to 1,000 h (~41 d) following PEC treatment, trending back toward baseline after 42 d. It remains to be determined which specific cell types or tissues orchestrate the immunometabolic shift observed in *B. schlosseri* following PEC. While the current bulk RNA-seq analysis identifies a systemic transition from inflammatory to regenerative signatures, future single-cell or spatial transcriptomic investigations will be required to resolve these cellular identities.

Discussion

The dramatic and persistent rejuvenating effect of PEC on aged *B. schlosseri* colonies strongly suggests a fundamental impact on their stem cells, which drive organismal aging in this species. Our prior work, using lineage tracing and transplantation, has isolated prospective stem cells, identified stem cell niches, and demonstrated the migration of both prospective germline and somatic stem cells from adult zooids into developing buds (17–19, 24, 39). These cells are essential contributors to the formation of new buds, as evidenced by the detection of chimerism and genotype takeover following the transplantation of a small number of enriched allogeneic stem cell populations between compatible colonies, as well as the observed differentiation of labeled enriched stem cells (17–19, 24, 39). Collectively, these studies suggest a crucial role of stem cells in *B. schlosseri* bud development and the maintenance of colonial integrity across asexual generations. Stem cell aging is a recognized feature in mammalian systems (45); for instance, hematopoietic stem cells (HSCs) expand with age, but exhibit a myeloid bias (my-HSC) (34, 35, 46). Depleting these my-HSCs restores a more youthful immune system (47). *B. schlosseri's* unique life cycle, where almost all tissues and differentiated cells, except for stem cells and hemocytes, are eliminated during weekly regeneration, makes stem cell aging the primary driver of observed organismal aging phenotypes. Our ability to maintain and document colonies for over 24 y, through more than 1,000 asexual cycles, further enhances its capacity as an exceptional chordate model for aging research. Our data show that PEC stimulation improves overall health and enhances budding and regeneration in both young and old *B. schlosseri* colonies. Nonpulsatile electrical (direct) stimulation is being reported to stimulate heart beats and siphon response in *Botryllus schlosseri* (48). The persistence of rejuvenation that we have observed through numerous asexual cycles in aged colonies suggests that the stimulus induces lasting alterations within their stem cell populations.

We found that PEC treatment induces a robust transcriptomic "reboot" characterized by an acute shift toward a stable, long-term rejuvenated baseline. These findings highlight a conservation of gene activation across colonies spanning a massive age gap including pathways associated with DNA/RNA stability, contractile integrity, and metabolic optimization.

Our transcriptomic gene regulation analyses suggest that PEC treatment functions as a nonmechanical surrogate for physical exercise. The acute "reboot and rebound" model in young colonies, defined by the 2-h suppression of contractile machinery followed by a 24-h surge in growth factors and metabolic activity, mirrors the biphasic response seen in human skeletal muscle following acute exercise. In humans, acute exercise induces a transient stress phase characterized by the immediate activation of metabolic sensors such as Nitric Oxide Synthase (*Nos*) (49). Our observation of acute *Nos1* and the *Gpcr Lphn2* up-regulation at 2 h indicates that PEC acts as a transducer of electric flux into similar chemical signals used during exercise to trigger downstream recovery and mitochondrial biogenesis (50, 51). A crucial component of the PEC-induced recovery is the sustained optimization of the mitochondrial and metabolic hub, which most likely functions as the bioenergetic engine for rejuvenation. At the 24-h peak, the up-regulation of *Idh3a* and *Ucp2* in young colonies points to a "metabolic surge" required to power energetically expensive tissue synthesis. This mirrors the metabolic shift seen in exercise, where mitochondrial enzymes are up-regulated to meet increased ATP demand (51). Specifically, the activation of *Ucp2* suggests an inhibition of mitochondrial superoxide production, preventing oxidative damage during rapid growth (52). This evolves into a long-term state of mitohormesis, where a nonlethal physiological stress triggers an adaptive response that enhances long-term mitochondrial health (53). The activation of protective transporters like *Abcg2* in both young and 20-y-old colonies (24 h), and the late-stage up-regulation of *Prdx4* (13 and 49 d) suggest that PEC treatment effectively "retrains" the mitochondrial network. By enhancing antioxidant capacity and metabolic efficiency, PEC might provide a long-term buffer against the bioenergetic decline that typically characterizes aged biological systems (54). This finding suggests that PEC stimulates mitochondrial "fitness" in a manner similar to that achieved through chronic endurance training (55, 56).

Aging is characterized by a global loss of heterochromatin and a decrease in linker histones, leading to genomic instability and "leaky" gene expression (57). The linker histone *H1f0* establishes transcriptional programs that restrict long-term proliferative potential and reduce phenotypic heterogeneity, effectively "locking" the

genome into a stable, differentiated state (58). We observed a sustained, late-stage upregulation of *H1f0* in both age groups. This suggests that the stimulus may act as a genomic "lock" to stabilize the rejuvenated phenotype long after the initial pulse. Furthermore, the activation of *H1f0* could represent a departure from the natural history of *B. schlosseri*, in which senescence is a strictly programmed, colony-specific event (30). By potentially reinforcing heterochromatin integrity, PEC treatment may provide a mechanism to bypass this programmed life span.

The proinflammatory to cell-repair signature transition following PEC stimulation suggests a role as a functional surrogate for physical exercise. This is most clearly demonstrated by the temporal shift transitioning from proinflammatory acute phase at 2 h posttreatment followed by tissue-reparative phenotype by 24 h. This biphasic response mirrors the activation patterns observed in humans and mice after physical exertion, as defined by the expression profiles of conserved gene sets associated with proinflammatory and reparative states (43, 44). In both mammalian exercise and colonial PEC treatment, the transcriptomic signature eventually stabilizes into a tissue-reparative phenotype, which serves to balance the initial inflammatory flux. The precise mechanisms linking brief electromagnetic stimulation to the effects of sustained physical activity remain to be elucidated., Despite being distinct interventions, exercise and PEC may promote systemic health and rejuvenation through convergent immunometabolic pathways.

Materials and Methods

Animal Culture, and Preparation. Mariculture procedures have previously been described (22). Briefly, *B. schlosseri* colonies were collected from the marina in Monterey or Santa Cruz, California. Individual colonies were tied to 3 × 5 cm glass slides and placed 5 cm away from and opposite another glass slide in a slide rack. The slide rack was placed into an aquarium, and within a few days, the sexually reproduced tadpoles hatched, swam to the settlement slide, metamorphosed into an oozoid, and matured into the adult body plan. Single colonies are then transferred to individual slides and grown at 18 to 20 °C and under 14 h/10 h light/dark regimen (6 a.m. to 8 p.m. light/8 p.m. to 6 a.m. dark). Colonies were fed daily using a marine invertebrate diet prepared in the lab as described in (22). Well-expanded colonies were split into 2 or more subclones and transferred to 2 or more slides, allowing the separate culture of genetically identical animals. Animals were taken for electrical stimulation in stage A and sampled for RNASeq or Flow cytometry analysis in stage A or early B. Colonies were considered to be young when less than 18 mo cultured on glass slides after initial settlement. The two aged colonies had been in continuous laboratory culture for 14 and 24 y, respectively, and were sampled throughout the four-year duration of this study (ages 12 to 14 for SC109e and 20 to 24 for 944).

ES Cell Differentiation. E14 ES cells were cultured using standard conditions (DMEM with 10% FCS (GibcoBRL ES cell qualified), 1,000 U/mL LIF (Chemikon), and fibroblast feeder cells from mouse embryos) (59). To obtain contracting cardiomyocytes, the cells were plated without feeders or LIF and allowed to grow for one to two weeks until beating cardiomyocyte patches were visible.

Pulsatile Electrical Stimulus. A Medtronic 5375 pulse generator (Medtronic, MN) was used to PEC-stimulate *Botryllus* colonies. Settings used are as indicated for individual experiments. Animals were routinely stimulated at 20 milliamps (ma) and 150 pulses per minute (ppm) for 5 min. This stimulation regimen was repeated three times at 15 to 20 min intervals. For some initial experiments, 20 mA, 150 ppm for 5 min was applied 6 times with 48-h intervals. Conditions of the stimulation setup are shown in *SI Appendix*, Fig. S1*A*. Briefly, leads with only the last 5 mm exposed were positioned on either side of colonies cultivated on glass and submerged in shallow autoclaved seawater sourced from Monterey Bay. The distance between the electrodes was approximately 1 cm (range 0.5 to 2 cm). Following stimulation, the animals were returned to their mariculture tanks. PEC treated animals and their controls were kept in separate tanks to accommodate the frequent removal from the tanks to score by microscope. PEC-treated and control-animals were removed from the tanks into Petri dishes for PEC treatment or scoring/photography with similar frequency and time. We did not notice any clear changes, even with longer PEC exposure (up to 16 h) other than the ones discussed in this paper.

Identification of *B. schlosseri* Aging Phenotypes. Morphological changes such as zooid and bud numbers and the presence or absence of gonads were recorded every 2 to 5 d during the initial phases following stimulation and monthly afterward. Colonies were assessed at least monthly until mortality, sampling, or the conclusion of the 4-y study period. Pictures and videos of young and old colonies were taken using a Zeiss V12 microscope/Canon camera or iPhone with an in-house produced phone holder and smartphone time lapse controller (Kiss-system https://github.com/TomRolander/KISS_Smartphone_Time-Lapse_Controller). Morphological changes were recorded (e.g., pigmentation level, blood vessel shape). Zooid sizes and ampullae length/width ratios were measured using Image J to measure the dorsal surface area, using a mm grid on the same photo to convert imageJ measurements to mm or mm^2. Heartbeat frequency was determined by analyzing videos of treated and control colonies, focusing on zooid heartbeats (Movies S1 and S2). A *t* test was used to find significant changes. Graphs were prepared using Graphpad Prism 10.6.1. Figures were prepared using Pixelmator Pro 3.7.1.

Flow Cytometry Analysis. Flow cytometry was performed on multiple colonies, both young and old, all in stage A or B at the time of harvest. Colonies were dissociated with a fine blade into cell suspensions for cell isolation. Cells were filtered through a 70-μm mesh followed by a 35-μm mesh using a sterile 1-mL syringe pump, washed, and collected in staining medium: M199 with 3.3 × HBSS. No enzymatic dissociation was used. Cells were resuspended in 1 mL of the staining media, and 1 μL of Alkaline Phosphatase Live Stain (ThermoFisher) was added. Cells were incubated for 30 min on ice under dark conditions, and 1 μL of Propidium Iodide (1 μg/mL) was added before flow analysis. After gating on propidium iodide (PI) negative cells (using 2D plots owing to the natural fluorescence of *B. schlosseri* cells), cells were analyzed using forward (FSC) and backscatter (BSC) on a log scale and fluorescence from Alkaline Phosphatase using a Sony MA900. Flow cytometry data were analyzed using Flowjo.

Sample-Collection for Sequence Analysis. Tissue samples were collected from *Botryllus schlosseri* colonies raised in the Hopkins Marine Station Mariculture Facility. They were left without food for 20 h prior to dissection to reduce non-*Botryllus* RNA. Colonies were frozen in liquid nitrogen and held at −80 °C prior to library preparation. Colonies were sampled from systems at stage A-B.

Library Preparation. RNA was prepared from frozen samples using Zymo Research Quick RNA MIcro Prep Kit # R1050 and cleaned using Zymo Research RNA Clean and Concentrator #R1015. Samples were analyzed on an Agilent QC 2100 Bioanalyzer to determine quality prior to library preparation. cDNA was prepared using the Nugen Ovation RNA Sequencing System V2, #7102, and cleaned using the QIAGEN QIAquick PCR purification kit, #28104, as recommended in the protocol and analyzed on the Agilent QC Bioanalyzer. If needed, samples were size-selected using Zymo Research Select-A-Size DNA Clean and Concentrator #D4080 prior to barcoding. The final library was prepared using NEB NEBNext Ultra II DNA Library Prep Kit #27645 and barcoded using NEBNext Multiplex Oligos for Illumina #E6609S. All magnetic bead purification was accomplished using BullDogBio CleanNGS RNA and DNA Spri Beads #CNGS005. Samples were then analyzed using the Agilent QC 2100 Bioanalyzer to determine the concentration of each sample prior to sequencing. On average, 12 million 2 × 150 bp reads (Illumina Nextseq 2000 P3) were sequenced for each library.

Transcriptome Analysis. To study molecular changes associated with rejuvenation, we pulsed young (373 to 465-d-olds) and old (7,668-d-old) colonies, generating comprehensive whole-transcriptome sequence data from 47 samples (*SI Appendix*, Supplement Data 2). Both PEC-treated and control colonies were sampled. Young colonies were sampled at 5 time points posttreatment: 2 h (n = 12), 24 h (n = 12), 13 and 49 d (n = 8), and 132 d (n = 6). Old colonies were sampled at 3 time points: 24 h (n = 5), 41 d, and 93 d (n = 5). All specimens were sampled at the same developmental stage, stage A. Control and Treated colonies per every time point were sampled on the same date. Bulk RNA-seq libraries were prepared and sequenced on an Illumina NextSeq 2000 P3 platform. Reads were

aligned to the *Botryllus* genome, and gene expression was measured as described in (22). Reads were trimmed (trim galore) and aligned to the *Botryllus* genome (14) using STAR (60). Gene count tables were created using HTseq. Samples with less than 10,000 total counts were removed. DEseq2 was used to identify differentially expressed genes with *P* value <= 0.05 and a Log fold change cutoff absolute value >1. Functional gene regulation groups Fig. 4 *A* and *B* are based on Gene Analytics analysis data (SI1).

Gene Orthology. Gene orthology is based on sequence similarities between the *B. schlosseri* gene models and human and mouse gene annotations (BLAST score smaller than e-10), as described in the *B. schlosseri* genome paper (14). All discussions regarding genes are based on sequence similarities alone.

Proimmune Versus Cell-Repair-Signature. The M1 (proimmune)/M2 (cell repair) macrophage polarization state analysis was done as previously described (43). In short, a previously identified macrophage gene set (44) of 338 genes, which accurately separated proimmune (M1) vs. cell-repair (M2) macrophages in both training and validation-independent clinically prescribed macrophage datasets (M1 = 48 genes, M2 = 290 genes), was used initially. Of those 338 genes, 112 had a homologous *Botryllus* gene. When multiple *Botryllus* Gene Identities (Gis) were homologous to the same gene, all such Gis were used, leading to 13 M1 Gis and 133 M2 Gis in the *Botryllus* analysis (SI1). A combined score was calculated from these genes. The genes within each cluster were initially normalized and then averaged to derive the score. The normalization of gene expression values followed a modified Z-score approach centered around the StepMiner threshold (formula = (expression – (SThr + 0.5))/3∗stdev) (60). A weighted linear combination of the cluster averages was employed to generate a score for each sample. Subsequently, the samples were organized based on this linearly combined score. The direction of the pathway was determined by the connection from an M1 cluster to an M2 cluster, with M1-associated genes being given a negative weight and M2-associated genes a positive weight. A noise margin for this composite score was computed, adhering to the same linearly weighted combined score with a 2-fold change allowance (±0.5 around the StepMiner threshold). In Fig. 4*C*, the scores for GSE27536 were calculated with only the M1-associated genes due to the disease status of all the samples in those datasets.

For the *Botryllus* control vs the 2 h-post-PEC treatment analysis, only the M1-associated genes were used to calculate the scores, as the PEC stimulus was also considered stress-inducing in the samples. The long-term (control vs 300 to 1,000 h and 1,000+ h) *Botryllus* analysis used both the M1 and M2 associated genes.

Data, Materials, and Software Availability. RNA-seq data have been deposited at the Sequence Read Archive (SRA) under BioProject PRJNA1219309 (42). The human and mouse exercise data have been published (43) and are publicly available with Gene Expression Omnibus ids: GSE104079 (61), GSE27536 (62), GSE120862 (63), GSE83578 (64), GSE111555 (65), GSE99963 (66), GSE144304 (67), and GSE28998 (68).

ACKNOWLEDGMENTS. We thank Stuart Thompson, Steve Palumbi, and Tal Raveh for helpful discussions. We are also grateful to Medtronic for supplying pacing materials and to the San Francisco CZ Biohub genomic personnel for their important contribution to the RNA sequencing. Gemini was used to assist with editing and grammar. This work was supported by a National Institute on Aging Grant 5RO1 AG076908 to A.V. and I.L.W.; Wu Tsai Human Performance Alliance (WTHPA) to Y.V. and D.S., Chan Zuckerberg San Francisco Biohub to A.V. and I.L.W., the Gruss Lipper Postdoctoral Fellowship to T.L., a Big Ideas for Oceans Grant from the Stanford Oceans Department and Stanford Woods Institute for the Environment, Bio-X and ISCBRM Stanford seed Grants to A.V.

Author affiliations: [a]Biology Department, Stanford University, Hopkins Marine Station, Pacific Grove, CA 93950; [b]Department of Pathology and Institute for Stem Cell Biology and Regenerative Medicine, Stanford University School of Medicine, Stanford, CA 94305; [c]Department of Bioinformatics and System Biology, Jacobs School of Engineering, University of California, San Diego, CA 92093; [d]Department of Integrative Biology, University of California, Berkeley, CA 94704; [e]Chan Zuckerberg Biohub SF, San Francisco CA 94158; [f]Department of Pediatrics, University of California, San Diego, CA 92093; and [g]Department of Computer Science and Engineering, Jacob's School of Engineering, University of California, San Diego, CA 92093

Author contributions: J.D., Y.V., T.L., E.M.D., I.L.W., K.L.G., D.S., and A.V. designed research; J.D., Y.V., T.L., E.M.D., K.J.I., K.J.P., C.A., N.F.N., K.L.G., and A.V. performed research; J.D., Y.V., T.R., N.F.N., A.M.D., K.L.G., D.S., and A.V. contributed new reagents/analytic tools; J.D., Y.V., E.M.D., K.J.I., K.L.G., and A.V. analyzed data; and J.D., Y.V., E.M.D., N.F.N., I.L.W., K.L.G., and A.V. wrote the paper.

1. M. Levin, Reprogramming cells and tissue patterning via bioelectrical pathways: Molecular mechanisms and biomedical opportunities. *Wiley Interdiscip. Rev. Syst. Biol. Med.* **5**, 657–676 (2013).
2. M. Levin, Bioelectric signaling: Reprogrammable circuits underlying embryogenesis, regeneration, and cancer. *Cell* **184**, 1971–1989 (2021).
3. J. L. Whited, M. Levin, Bioelectrical controls of morphogenesis: From ancient mechanisms of cell coordination to biomedical opportunities. *Curr. Opin. Genet. Dev.* **57**, 61–69 (2019).
4. E. Lagasse, M. Levin, Future medicine: From molecular pathways to the collective intelligence of the body. *Trends Mol. Med.* **29**, 687–710 (2023).
5. B. Oh *et al.*, Electrical modulation of transplanted stem cells improves functional recovery in a rodent model of stroke. *Nat. Commun.* **13**, 1366 (2022).
6. B. A. Karamian *et al.*, The role of electrical stimulation for rehabilitation and regeneration after spinal cord injury. *J. Orthop. Traumatol.* **23**, 2 (2022).
7. L. Ni *et al.*, Electrical stimulation therapy for peripheral nerve injury. *Front. Neurol.* **14**, 1081458 (2023).
8. E. Braun, H. Ori, Electric-induced reversal of morphogenesis in *Hydra*. *Biophys. J.* **117**, 1514–1523 (2019).
9. Y. Wang, Y. Ma, Q. Zhong, B. Song, Q. Liu, Transcriptomic analysis of rat brain response to alternating current electrical stimulation: unveiling insights via single-nucleus RNA sequencing. *MedComm* **5**, e514 (2024).
10. T. E. Shin *et al.*, Motility enhancement of human spermatozoa using electrical stimulation in the nano-ampere range with enzymatic biofuel cells. *PLoS One.* **15**, e0228097 (2020).
11. Y. J. Cheah, M. R. Buyong, M. H. Mohd Yunus, Wound healing with electrical stimulation technologies: A review. *Polymers* **13**, 3790 (2021).
12. R. Das *et al.*, Electrical stimulation for immune modulation in cancer treatments. *Front. Bioeng. Biotechnol.* **9**, 795300 (2021).
13. S. Roy Barman, S. Jhunjhunwala, Electrical stimulation for immunomodulation. *ACS. Omega* **9**, 52–66 (2024).
14. A. Voskoboynik *et al.*, The genome sequence of the colonial chordate. *Botryllus schlosseri*. *Elife* **2**, e00569 (2013).
15. F. Delsuc, H. Brinkmann, D. Chourrout, H. Philippe, Tunicates and not cephalochordates are the closest living relatives of vertebrates. *Nature* **439**, 965–968 (2006).
16. V. L. Scofield, J. M. Schlumpberger, L. A. West, I. L. Weissman, Protochordate allorecognition is controlled by a MHC-like gene system. *Nature* **295**, 499–502 (1982).
17. D. J. Laird, A. W. De Tomaso, I. L. Weissman, Stem cells are units of natural selection in a colonial ascidian. *Cell* **123**, 1351–1360 (2005).
18. A. Voskoboynik *et al.*, Identification of the endostyle as a stem cell niche in a colonial chordate. *Cell Stem Cell* **3**, 456–464 (2008).
19. Y. Rinkevich *et al.*, Repeated, long-term cycling of putative stem cells between niches in a basal chordate. *Dev. Cell* **24**, 76–88 (2013).
20. A. Voskoboynik *et al.*, Identification of a colonial chordate histocompatibility gene. *Science* **341**, 384–387 (2013).
21. L. Manni *et al.*, Sixty years of experimental studies on the blastogenesis of the colonial tunicate *Botryllus schlosseri*. *Dev. Biol.* **448**, 293–308 (2019).
22. M. Kowarsky *et al.*, Sexual and asexual development: Two distinct programs producing the same tunicate. *Cell Rep.* **34**, 108681 (2021).
23. L. Ballarin *et al.*, Stem cells and innate immunity in aquatic invertebrates: Bridging two seemingly disparate disciplines for new discoveries in biology. *Front. Immunol.* **12**, 688106 (2021).
24. T. Levy *et al.*, Germline stem cell isolation, lineage tracing, and aging in a protochordate. bioRxiv [Preprint] (2024), 10.1101/2025.08.31.673173 (Accessed 3 September 2025).
25. A. Voskoboynik, I. L. Weissman, An emerging model for the study of aging, stem cells, and mechanisms of regeneration. *Invertebr. Reprod. Dev.* **59**, 33–38 (2015).
26. C. Anselmi *et al.*, Two distinct evolutionary conserved neural degeneration pathways characterized in a colonial chordate. *Proc. Natl. Acad. Sci. U.S.A.* **119**, e2203032119 (2022).
27. Y. Voskoboynik *et al.*, Global age-specific patterns of cyclic gene expression revealed by tunicate transcriptome atlas. bioRxiv [Preprint] (2020), https://doi.org/10.1101/2020.12.08.417055.
28. D. S. Stoner, B. Rinkevich, I. L. Weissman, Heritable germ and somatic cell lineage competitions in chimeric colonial protochordates. *Proc. Natl. Acad. Sci. U.S.A.* **96**, 9148–9153 (1999).
29. D. S. Stoner, I. L. Weissman, Somatic and germ cell parasitism in a colonial ascidian: Possible role for a highly polymorphic allorecognition system. *Proc. Natl. Acad. Sci. U.S.A.* **93**, 15254–15259 (1996).
30. B. Rinkevich, R. J. Lauzon, B. W. Brown, I. L. Weissman, Evidence for a programmed life span in a colonial protochordate. *Proc. Natl. Acad. Sci. U.S.A.* **89**, 3546–3550 (1992).
31. I. L. Weissman, Stem cells are units of natural selection for tissue formation, for germline development, and in cancer development. *Proc. Natl. Acad. Sci. U.S.A.* **112**, 8922–8928 (2015).
32. I. L. Weissman, Stem cells: Units of development, units of regeneration, and units in evolution. *Cell* **100**, 157–168 (2000).
33. H. Ueno, B. B. Turnbull, I. L. Weissman, Two-step oligoclonal development of male germ cells. *Proc. Natl. Acad. Sci. U.S.A.* **106**, 175–180 (2009).
34. I. Beerman *et al.*, Functionally distinct hematopoietic stem cells modulate hematopoietic lineage potential during aging by a mechanism of clonal expansion. *Proc. Natl. Acad. Sci. U.S.A.* **107**, 5465–5470 (2010).
35. D. J. Rossi, C. H. M. Jamieson, I. L. Weissman, Stems cells and the pathways to aging and cancer. *Cell* **132**, 681–696 (2008).
36. M. Jan *et al.*, Clonal evolution of preleukemic hematopoietic stem cells precedes human acute myeloid leukemia. *Sci. Transl. Med.* **4**, 149ra118 (2012).
37. S. Jaiswal *et al.*, CD47 is upregulated on circulating hematopoietic stem cells and leukemia cells to avoid phagocytosis. *Cell* **138**, 271–285 (2009).
38. L. Ballarin, F. Schiavon, L. Manni, Natural apoptosis during the blastogenetic cycle of the colonial ascidian *Botryllus schlosseri*: A morphological analysis. *Zoolog. Sci.* **27**, 96–102 (2010).

39. B. Rosental *et al.*, Complex mammalian-like haematopoietic system found in a colonial chordate. *Nature* **564**, 425–429 (2018).
40. M. D. O'Connor *et al.*, Alkaline Phosphatase-Positive colony formation is a sensitive, specific, and quantitative indicator of undifferentiated human embryonic stem cells. *Stem Cells* **26**, 1109–1116 (2008).
41. L. Ballarin *et al.*, Haemocytes and blastogenetic cycle in the colonial ascidian *Botryllus schlosseri*: A matter of life and death. *Cell Tissue Res.* **331**, 555–564 (2008).
42. Y. Voskoboynik, Electrical stimulation promotes longevity and regeneration in a colonial chordate. BioProject. https://dataview.ncbi.nlm.nih.gov/object/PRJNA1219309. Deposited 4 February 2025.
43. Y. Voskoboynik, A. D. McCulloch, D. Sahoo, Macrophages on the run: Exercise balances macrophage polarization for improved health. *Mol. Metab.* **90**, 102058 (2024).
44. P. Ghosh *et al.*, Machine learning identifies signatures of macrophage reactivity and tolerance that predict disease outcomes. *EBioMedicine* **94**, 104719 (2023).
45. C. López-Otín, M. A. Blasco, L. Partridge, M. Serrano, G. Kroemer, Hallmarks of aging: An expanding universe. *Cell* **186**, 243–278 (2023).
46. W. W. Pang *et al.*, Human bone marrow hematopoietic stem cells are increased in frequency and myeloid-biased with age. *Proc. Natl. Acad. Sci. U.S.A.* **108**, 20012–20017 (2011).
47. J. B. Ross *et al.*, Depleting myeloid-biased haematopoietic stem cells rejuvenates aged immunity. *Nature* **628**, 162–170 (2024).
48. C. Anselmi *et al.*, Direct current stimulation (DCS) modulates gene expression related to human diseases in the marine chordate *Botryllus schlosseri*. *Neurobiol. Dis.* **221**, 107314 (2026).
49. J. L. Areta *et al.*, Timing and distribution of protein ingestion during prolonged recovery from resistance exercise alters myofibrillar protein synthesis. *J. Physiol.* **591**, 2319–2331 (2013).
50. B. Egan, J. R. Zierath, Exercise metabolism and the molecular regulation of skeletal muscle adaptation. *Cell Metab.* **17**, 162–184 (2013).
51. M. D. Brand, T. C. Esteves, Physiological functions of the mitochondrial uncoupling proteins UCP2 and UCP3.. *Cell Metab.* **2**, 85–93 (2005).
52. M. Ristow, K. Schmeisser, Mitohormesis: Promoting health and lifespan by increased levels of reactive oxygen species (ROS). *Dose Response* **12**, 288–341 (2014).
53. C. López-Otín, M. A. Blasco, L. Partridge, M. Serrano, G. Kroemer, The hallmarks of aging. *Cell* **153**, 1194–1217 (2013).
54. M. Granath-Panelo, S. Kajimura, Mitochondrial heterogeneity and adaptations to cellular needs. *Nat. Cell Biol.* **26**, 674–686 (2024).
55. W. R. Hood *et al.*, The mitochondrial contribution to animal performance, adaptation, and life-history variation. *Integr. Comp. Biol.* **58**, 480–485 (2018).
56. R. J. O'Sullivan, S. Kubicek, S. L. Schreiber, J. Karlseder, Reduced histone biosynthesis and chromatin changes arising from a damage signal at telomeres. *Nat. Struct. Mol. Biol.* **17**, 1218–1225 (2010).
57. C. M. Torres *et al.*, The linker histone H1.0 generates epigenetic and functional intratumor heterogeneity.. *Science* **353**, aaf1644 (2016).
58. J. P. Fisher, S. A. Hope, M. L. Hooper, Factors influencing the differentiation of embryonal carcinoma and embryo-derived stem cells. *Exp. Cell Res.* **182**, 403–414 (1989).
59. A. Dobin, T. R. Gingeras, Mapping RNA-seq reads with STAR. *Curr. Protoc. Bioinform.* **51**, 11.14.1–11.14.19 (2015).
60. D. Sahoo, D. L. Dill, R. Tibshirani, S. K. Plevritis, Extracting binary signals from microarray time-course data. *Nucleic Acids Res.* **35**, 3705–3712 (2007).
61. K. Marosi *et al.*, Metabolic and molecular framework for the enhancement of endurance by intermittent fasting. Gene Expression Omnibus. https://www.ncbi.nlm.nih.gov/geo/query/acc.cgi?acc=GSE104079. Accessed 21 September 2022.
62. N. Turan *et al.*, Vastus lateralis biopsies from healthy and COPD patients before and after 8 weeks of exercise training. Gene Expression Omnibus. https://www.ncbi.nlm.nih.gov/geo/query/acc.cgi?acc=GSE27536. Accessed 21 September 2022.
63. D. V. Popov *et al.*, Contractile activity-specific transcriptome response to acute endurance exercise and training in human skeletal muscle. Gene Expression Omnibus. https://www.ncbi.nlm.nih.gov/geo/query/acc.cgi?acc=GSE120862. Accessed 20 September 2022.
64. A. Abbasi *et al.*, Sex-specific variation in signaling pathways and gene expression patterns in human leukocytes in response to endotoxin and exercise. Gene Expression Omnibus. https://www.ncbi.nlm.nih.gov/geo/query/acc.cgi?acc=GSE83578. Accessed 7 December 2021.
65. J. L. da Silva *et al.*, Blood and skeletal muscle gene signatures of exercise training in men. Gene Expression Omnibus. https://www.ncbi.nlm.nih.gov/geo/query/acc.cgi?acc=GSE111555. Accessed 11 October 2022.
66. R. C. Laker *et al.*, Transcriptomic and epigenetic responses to short-term nutrient-exercise stress in humans [RNA-seq]. Gene Expression Omnibus. https://www.ncbi.nlm.nih.gov/geo/query/acc.cgi?acc=GSE99963. Accessed 8 February 2023.
67. M. D. van der Hoek *et al.*, Muscle function in fit and (pre-)frail males and females. Gene Expression Omnibus. https://www.ncbi.nlm.nih.gov/geo/query/acc.cgi?acc=GSE144304. Accessed 9 June 2024.
68. P. Gordon *et al.*, Human skeletal muscle transcriptional response to exercise. Gene Expression Omnibus. https://www.ncbi.nlm.nih.gov/geo/query/acc.cgi?acc=GSE28998. Accessed 7 February 2023.